CHAPTER 3

COMPONENT DESCRIPTION AND MODELING

The purpose of this Chapter is to provide a detailed description of the EMS and the analytical and numerical modeling methods use to predict the performance of individual components of the EMS; these are the size selective inlet, the particle charger, the mobility classifier, the electrometer and the data acquisition and processing system. The first Section gives the detailed description and the analytical model of a size selective inlet. The second Section provides the detailed description of the particle chargers and the electrostatic characteristics of the unipolar corona charger including the semi-empirical method used to predict the product of the ion concentration and charging residence time in the charging zone of the charger, the analytical theories used to estimate the particle penetration and charging rate of the charger, and the numerical model developed to investigate the flow and electric fields in the charging zone of the charger, while the third Section presents the detailed description of the mobility classifier and the analytical and numerical models used to predict the landing location of the charged particle along the mobility classifier, the mobility and size classification of the particles that land on the different electrometer rings along the classifier, and flow field and electric field patterns in the classifier. In the fourth Section, the detailed description and the analytical model of the electrometer circuit are presented. The last Section of the Chapter describes the data acquisition of the spectrometer and show how to calculate the particle size distribution of aerosols.

3.1 Size Selective Inlet

3.1.1 Description

The inertial impactor was used to remove particles outside the measurement size range upstream of the EMS based on their aerodynamic diameter. The aerodynamic diameter at which the particles are separated is called the cut-point diameter. A schematic diagram of the size selective inlet used in this study is shown in Figure 3.1. It consists of an acceleration nozzle and an impaction plate. The acceleration nozzle and the impaction plate are made of a stainless steel. For the size selective inlet detailed drawings are provided in Appendix A.1. In inertial impactor, the aerosol flow is accelerated through an acceleration nozzle 1.0 mm in diameter directed at an impaction plate. The distance from the acceleration nozzle to the impaction plate is a 1.0 mm in diameter. The impaction plate deflects the flow streamlines to a 90° bend. Particles with sufficient inertia are unable to follow the streamlines and impact on the collection plate. Smaller particles are able to follow the streamlines and avoid contact with the plate and exit the impactor. The impactor used in this study has a particle cut-point diameter is 1.28 μm for aerosol flow rate of 2.0 l/min. Figure 3.2 shows a picture of the inertial impactor used in the present study.

3.1.2 Analytical Model

The acceleration nozzle diameter can be calculated from the Stokes number (Stk). The Stokes number is a dimensionless parameter that characterizes impaction. The Stokes number equation for a round jet impactor is defined as follows (Hinds 1999):

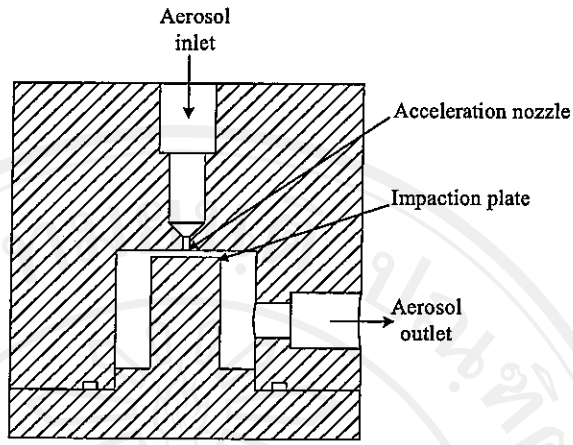

Figure 3.1 Schematic diagram of the size selective inlet.

Figure 3.2 A picture of the inertial impactor.

$$\text{Stk}=\frac{\rho_p C_c d_p^2 U}{9\eta D} \tag{3.1}$$

where ρ_p is the particle density, C_c is the Cunningham slip correction factor, d_p is the particle cut-point diameter, U is the mean velocity at the throat, η is the gas viscosity, and D is the acceleration nozzle diameter. For the round jet impactor, the expression of the average velocity within the round jets is given by following equation

$$U=\frac{4Q}{\pi D^2} \tag{3.2}$$

Substituting Equation 3.2 into Equation 3.1 gives

$$\text{Stk}=\frac{4\rho_p C_c d_p^2 Q}{9\pi\eta D^3} \tag{3.3}$$

Solving the above equation for the particle cut-point diameter at 50% collection efficiency, d_{50}, can be calculated by (Hinds 1999)

$$d_{50}\sqrt{C_c} = \sqrt{\frac{9\pi\eta D^3 \mathrm{Stk}_{50}}{4\rho_p Q}} \tag{3.4}$$

Because C_c is a function of d_{50}, Equation 3.4 cannot be conveniently solved for particle diameter. For conventional impactor, d_{50} can be estimated from $d_{50}\sqrt{C_c}$ using the following empirical equations (Hinds 1999)

$$d_{50} = d_{50}\sqrt{C_c} - 0.078\times10^{-8} \qquad \text{for } d_{50} \text{ in m} \tag{3.5}$$

This equation is accurate within 2% for $d_{50} > 0.2$ μm and pressure from 0.9 – 1 atm (Hinds 1999). Thus, the acceleration nozzle diameter is given by

$$D = \sqrt[3]{\frac{4\rho_p \left(d_{50}\sqrt{C_c}\right)^2 Q}{9\pi\eta \mathrm{Stk}_{50}}} \tag{3.6}$$

where Stk_{50} is the Stokes number of a particle having a 50% collection efficiency. For the round jet impactor, Stk_{50} is 0.24 (Hinds 1999), and the ratio of the acceleration nozzle diameter to the nozzle-to-plate distance is 1.0 (Marple and Willeke 1976). The mathematical expression for the collection efficiency (E) of the inertial impactor is determined as follows (Marjamaki *et al.* 2000)

$$E = \left[1 + \left(\frac{d_{50}}{d_p}\right)^{2s}\right]^{-1} \tag{3.7}$$

where s is the parameter affecting the steepness of the collection efficiency curve. In the present study, $s = 1$ is arbitrarily assumed for the steepness of the collection efficiency curve.

3.2 Particle Charger

3.2.1 Description

Two types of chargers are considered in this study. Both particle chargers are based on an electrical discharge generated between a corona-electrode and an outer electrode which is grounded. The corona discharge generates ions which move rapidly in the strong corona discharge field toward the outer electrode wall. Aerosol flow is directed across the corona discharge field and is charged by ion-particle collisions via diffusion charging and field charging mechanisms. In this study, both needle and wire-cylinder corona chargers were constructed and compared. Figure 3.3 shows a schematic diagram of the corona-needle charger used in the present study (detailed drawings are provided in Appendix A.2). The corona-needle charger's geometrical configuration is similar to the charger used by Hernandez-Sierra *et al.* (2003) and Alonso *et al.* (2005). It consists of a coaxial corona-needle electrode placed along the axis of a cylindrical tube with tapered ends. The needle electrode is made of a stainless steel rod 3 mm in diameter and 49 mm in length, ending in a sharp tip. The angle of the needle cone was about 9° and the tip radius was about 50 μm, as estimated under a microscope. The outer cylindrical is made of aluminum tube 30 mm in diameter and 25 mm in length with conical shape.

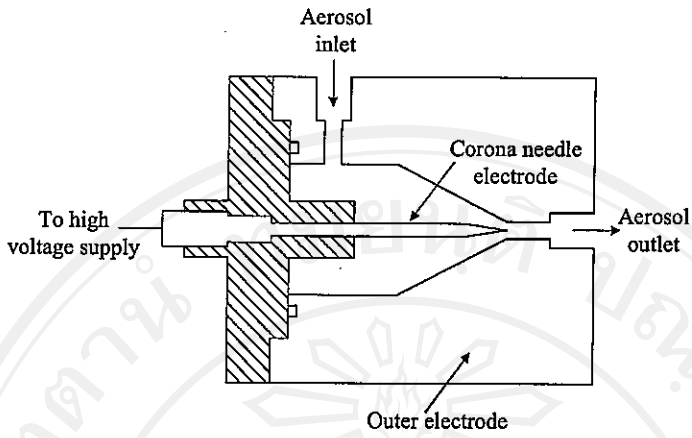

Figure 3.3 Schematic diagram of the corona-needle charger.

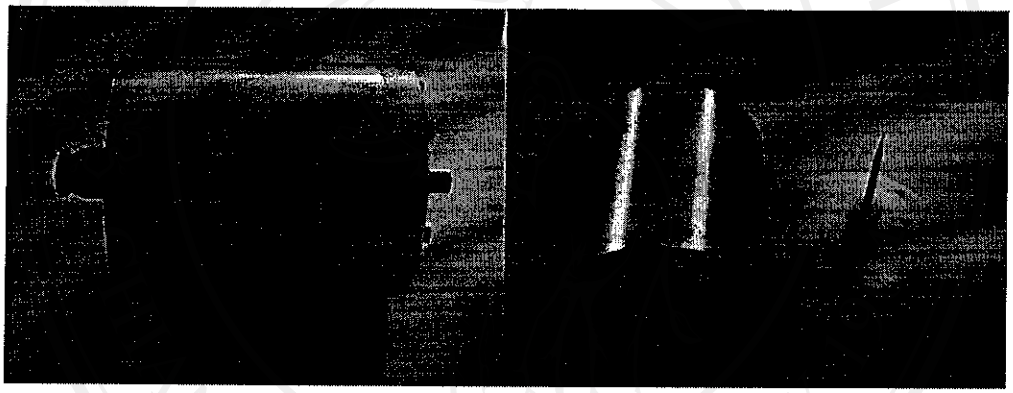

Figure 3.4 A picture of the corona-needle charger.

The angle of the cone was about 30° and the orifice diameter was about 4 mm. The distance between the needle electrode and the cone apex is 2 mm. The corona electrode head is connected to a DC high voltage supply, while the outer electrode is grounded. An adjustable DC high voltage power supply is used to maintain the corona voltage difference, typically of the order of 2.0 – 5.0 kV. Figure 3.4 shows a picture of the corona-needle charger. A schematic diagram of the corona-wire charger used in this study is shown in Figure 3.5 (detailed drawings are provided in Appendix A.3). It has a geometrical configuration similar to that used by Lethtimaki (1987) and Keskinen *et al.* (1992). It consists of a coaxial corona-wire electrode placed along the axis of a metallic cylinder tube. The outer electrode is made of aluminum tube 28 mm in diameter and 10 mm in length. The corona-wire electrode is made of stainless steel wire 300 μm in diameter and 10 mm in length. DC high voltage supply is used to produce the corona discharge on the wire electrode, typically in the range between 7.0 – 10.0 kV, while the outer metallic electrode is grounded. Figure 3.6 shows a picture of the corona-wire charger.

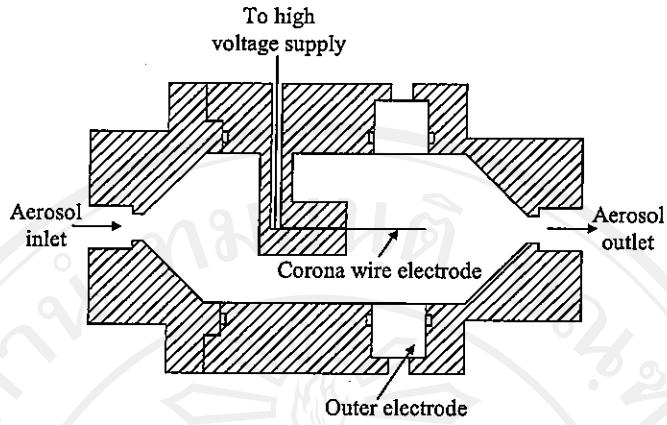

Figure 3.5 Schematic diagram of the corona-wire charger.

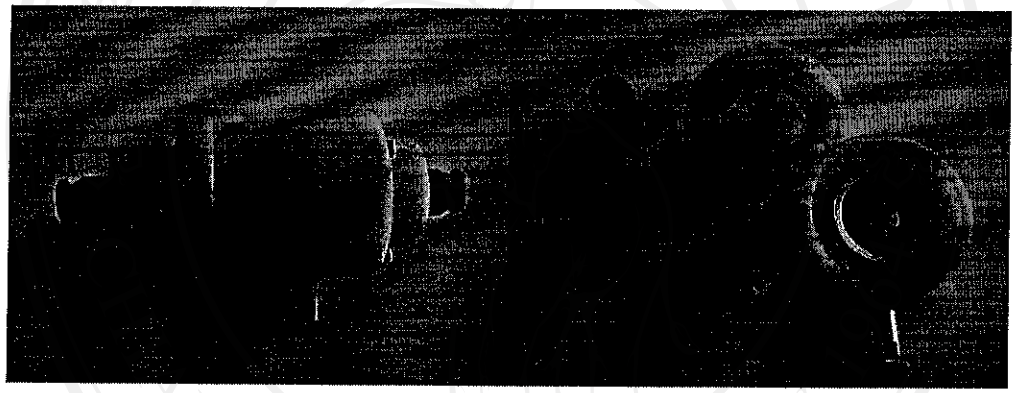

Figure 3.6 A picture of the corona-wire charger.

3.2.2 Analytical Models

In this Section, the electrostatic properties in terms of voltage-current relationships of both needle and wire-cylinder corona chargers are compared and evaluated for positive and negative coronas at different operating conditions. A semi-empirical method was used based on ion current measurement and electrostatic charging theory. Average and spatial distribution of ion concentrations in the charging region of the corona charger were calculated. The space charge effect was also considered. Finally, distribution of the $N_i t$ product as well as particle penetration and average elementary charge on particle against its diameter were computed and discussed.

(a) Spatial distribution of ion concentration

Derivation of the theoretical current-voltage relation proceeds from Poisson's equation which governs all electrostatic phenomena and is given by the following equation

$$\nabla^2 V = -\frac{\rho}{\varepsilon_0} \tag{3.8}$$

where V is the applied voltage, ρ is the space-charge density, and ε_0 is the vacuum permittivity (8.854×10^{-12} F/m). Assuming no axial variation, the above equation can be expressed in cylindrical coordinates as

$$\frac{1}{r}\frac{dV}{dr}\left(r\frac{dV}{dr}\right)+\frac{\rho(r)}{\varepsilon_0}=0 \tag{3.9}$$

Considering that the ion current density is

$$\vec{j}=\rho\vec{u}_i \tag{3.10}$$

where $u_i(r)=Z_iE(r)$ is the mean ionic velocity, Z_i is the electrical mobility of the ions, $E(r)$ is the electric field is a function of radial position. The space-charge density can be expressed on the basis of the ion current, I_{ion}, through the inner surface area, A, of the outer electrode of the charger as

$$\rho(r)=\frac{I_{ion}}{Z_iE(r)A} \tag{3.11}$$

For the simplified cylindrical corona geometry, the space-charge density is given by

$$\rho(r)=\frac{I_{ion}}{2\pi rLZ_iE(r)} \tag{3.12}$$

where:

$$E(r)=-\frac{dV}{dr} \tag{3.13}$$

Noting that $j=\frac{I_{ion}}{2\pi rL}$. Here I_{ion} is the measured ion current at distance r from the corona-electrode in the charger with charging length L. Substituting $\rho(r)$ and $E(r)$ into Equation 3.9 gives

$$rE(r)\frac{dE(r)}{dr}+E(r)^2-\frac{I_{ion}}{2\pi L\varepsilon_0Z_i}=0 \tag{3.14}$$

This equation is readily integrated to

$$E(r)=\sqrt{\frac{I_{ion}}{2\pi L\varepsilon_0Z_i}+\frac{c}{r^2}} \tag{3.15}$$

This describes the electric field under space charge conditions where c is the integration constant which is constrained to the interval

$$-\frac{I_{ion}}{2\pi\varepsilon_0 L Z_i} r_1^2 \le c \le \left(\frac{V}{\ln(r_2/r_1)}\right)^2 \tag{3.16}$$

The space charge can, at most, compensate the electric field at the inner electrode to zero. The limiting case, $E(r_1) = 0$, corresponds to the lower limit for c. The other extreme of no space charge implies that $I_{ion} = 0$ and the expression for the electric field in a concentric electrode gap, if the space charge effect is neglected, is determined by

$$E(r) = \frac{V}{r \ln(r_2/r_1)} \tag{3.17}$$

Inserting $E(r)$ in Equation 3.15 gives the upper limit for c. The integral Equation 3.15 along the radial distance in the charging region of the charger is equal to the voltage difference

$$V = \int_{r_1}^{r_2} E(r)dr \tag{3.18}$$

The integration limits for the case of the ion generation zone are the corona-wire, r_1, and the outer electrode, r_2, radii, respectively. In the same way, V is the potential difference between the corona-wire electrode and the outer electrode of the charger. Integrating the above equation results in

$$V = \left| \sqrt{\frac{I_{ion}}{2\pi L\varepsilon_0 Z_i} r^2 + 2c} + \frac{c}{\sqrt{2c}} \ln \frac{\sqrt{\frac{I_{ion}}{2\pi L\varepsilon_0 Z_i} r^2 + 2c} - \sqrt{2c}}{\sqrt{\frac{I_{ion}}{2\pi L\varepsilon_0 Z_i} r^2 + 2c} + \sqrt{2c}} \right|_{r_1}^{r_2} \quad \text{for } c > 0 \tag{3.19}$$

$$V = \left| \sqrt{\frac{I_{ion}}{2\pi L\varepsilon_0 Z_i} r^2 + 2c} + \frac{c}{\sqrt{-2c}} \arccos \frac{1}{r} \sqrt{-\frac{4c\pi\varepsilon_0 L Z_i}{I_{ion}}} \right|_{r_1}^{r_2} \quad \text{for } c < 0 \tag{3.20}$$

The electric field strength at the surface of the corona-electrode at corona discharge onset, E_0, has been experimentally evaluated by Peek (1929) and fitted empirically by relation as

$$E_0 = E_s\left(\delta + A\sqrt{\delta/r_1}\right) \tag{3.21}$$

where:

$$\delta = \frac{T_r}{T}\frac{P}{P_r}, \tag{3.22}$$

E_s denotes the breakdown field in air at normal conditions (3.10×10^6 V/m for negative corona, and 3.37×10^6 V/m for positive corona, at standard temperature and pressure), A is a dimensioned constant (0.0308 $m^{1/2}$ for negative corona, and 0.0241 $m^{1/2}$ for positive corona),

δ is the relative density of air relative to normal conditions, T_r is the absolute temperature of room air, P_r is the normal atmosphere pressure, and T and P are the operating temperature and pressure of the air. If space-charge effect is neglected, the corona onset voltage V_0 can be calculated from Equation 3.17 as

$$V_0 = E_0 r_1 \ln(r_2/r_1) \tag{3.23}$$

The average ion current density j_{ion} at the outer electrode surface area as a function of the voltage at the corona discharge electrode, can be expressed by:

$$j_{ion} = \frac{4\varepsilon_0 Z_i}{r_2^3 \ln(r_2/r_1)} V(V - V_0) \tag{3.24}$$

This approximation was originally proposed by Townsend (1915). The ion current density in Equation 3.24 can be expressed in term of the ion current I_{ion} toward the inner surface of the outer electrode surface area of the charger as

$$I_{ion} = \frac{8\pi L\varepsilon_0 Z_i}{r_2^2 \ln(r_2/r_1)} V(V - V_0) \tag{3.25}$$

Assuming that the distortion of the field distribution due to the ion space charge effect is neglected, the ion current of Equation 3.25 is equal to

$$I_{ion} = 2\pi r_2 LneZ_i E(r) \tag{3.26}$$

where e is the value of elementary charge on an electron, and n is the ion density is expressed by

$$n = \begin{cases} \frac{4\varepsilon_0}{er_2^2}(V - V_0) & \text{for } V > V_0, \\ 0 & \text{for } V \le V_0. \end{cases} \tag{3.27}$$

It is clear that calculation of the ion current from voltage difference at the corona discharge electrode depends on the assumption of the ion properties. Although the exact physicochemical mechanism of the formation of the ions in corona discharges is not well known, there is evidence that primary ions formed in the corona region undergo a process of clustering reactions to produce ions of higher molecular weight (Pui 1976). It has been suggested that the average value for the positive and negative ion electrical mobility at atmospheric pressure were $Z_i^+ = 1.4 \times 10^{-4}$ m^2/V s and $Z_i^- = 2.2 \times 10^{-4}$ m^2/V s, respectively (White 1963). These are the average mobilities used throughout the calculations presented in this paper. For pressure other than atmospheric, and assuming no temperature variations, the electrical mobility of the ions is corrected by

$$Z_{i,p} = Z_i \frac{P}{P_r} \tag{3.28}$$

where $Z_{i,P}$ is the electrical mobility of the ions at pressure P, and P and P_r are the operating and reference pressure of the charger, respectively.

(b) Estimation of the $N_i t$ product of the Charger

The particle charging performance depends on the product of the ion concentration N_i and the mean residence time t of the particles to the ions in the charger. This $N_i t$ product is the main charging parameter. Therefore, prior to any modeling of the charging process, it is necessary to estimate the $N_i t$ product established in the charging zone under any operating conditions (corona voltages, sample flow rates, and operating pressure). The space-charge density can be defined in terms of the ion concentration, N_i , is

$$\rho = N_i e \tag{3.29}$$

Substituting into Equation 3.11, the ion number concentration in the charging zone of the charger in the absence of aerosol particles is given by

$$N_i(r) = \frac{I_{ion}}{eZ_i E(r) A} \tag{3.30}$$

For the corona-needle charger used in the present study, the inner surface area of the metallic cone (charger outlet) where the ion current is collected, and is given by

$$A = \pi (r_1 + r_2)\sqrt{(r_1 - r_2)^2 + L^2} \tag{3.31}$$

where r_1 and r_2 are the inner and outer radii of a conical-frustum, and L is the length of the charging zone. If the space charge effect is neglected, the electric field strength is assumed to be given by the simplified equation (This is actually a very rough estimation because neither space charge nor the high non-uniformity of the electric field near the electrode tip have been considered)

$$E = \frac{V}{d} \tag{3.32}$$

where V is the applied voltage, and d is the distance between the electrode tip and the cone apex. Substituting Equation 3.31 and 3.32 into Equation 3.30, the mean ion number concentration is given by

$$N_i = \frac{I_{ion} d}{eZ_i V \pi (r_1 + r_2)\sqrt{(r_1 - r_2)^2 + L^2}} \tag{3.33}$$

The mean aerosol residence time of the particles in the charging zone of this charger is given by

$$t = \frac{\pi L\left(r_1^2 + r_1 r_2 + r_2^2\right)}{3Q_a} \frac{P}{P_r} \tag{3.34}$$

where Q_a is the aerosol flow rate. For the standard aerosol flow of 5.0 l/min, the mean aerosol residence time in the charging zone is 0.0814 s at atmospheric pressure. For the corona-wire charger used in the present study, the inner surface area of the outer electrode of the charger is given by

$$A = 2\pi rL \tag{3.35}$$

If the space charge effect is neglected, the electric field strength, E, in the charging zone is given by Gauss's law,

$$E = \frac{V}{r \ln(r_2/r_1)} \tag{3.36}$$

where r_1 and r_2 are radii of the corona-wire and outer electrode, respectively. In the same way, substituting Equation 3.35 and 3.36 into Equation 3.30, the mean ion concentration is given by

$$N_i = \frac{I_{ion} \ln(r_2/r_1)}{2\pi L e Z_i V} \tag{3.37}$$

Assuming since the obstruction of the flow caused by the wire electrode is neglected due to the very thin ($r_1 << r_2$) wire electrode. Therefore, the mean residence time of particles in the charging zone of the corona-wire charger is equal to

$$t = \frac{\pi r_2^2 L}{Q_a} \frac{P}{P_r} \tag{3.38}$$

For the standard aerosol flow of 5.0 l/min, the mean aerosol residence time in the charging zone is 0.074 s at atmospheric pressure.

In calculation of variation of the particle residence time along the radial distance in the charging region, the flow velocity profile has to be taken into account. The parabolic velocity profile $u(r)$ for stationary laminar flow through the charger was assumed since the obstruction of the flow caused by the wire electrode is neglected due to the very thin ($r_1 << r_2$) wire electrode. The expression for the velocity profile is given, using "flow in a pipe" approximation, as (Janna 1993)

$$u(r) = -\frac{dp}{dz}\frac{r_2^2}{4\mu}\left(1 - \frac{r^2}{r_2^2}\right) \tag{3.39}$$

where μ is the viscosity of the gas and dp/dz is the constant pressure gradient is given by the following equations

$$\frac{dp}{dz} = -\frac{\rho \bar{U}^2 f}{4r_2} \tag{3.40}$$

where:

$$f = \frac{64}{\mathrm{Re}}, \tag{3.41}$$

$$\mathrm{Re} = \frac{2r_2\bar{U}\rho}{\mu}, \tag{3.42}$$

f is the friction factor, $\bar{U}$ is the mean axial flow velocity, ρ is the gas density and Re is the Reynolds number in the flow in a pipe. Thus, the charging residence time with the parabolic velocity profile is given by

$$t(r) = \frac{L}{u(r)} \tag{3.43}$$

(c) Estimation of the average charge

As described in Section 2.3, the diffusion charge, n_{diff}, can be calculated approximately using the following White's equation for the number of diffusion charges acquired in time, t, is given by

$$n_{\mathrm{diff}} = \frac{d_p kT}{2K_E e^2} \ln\left(1 + \frac{\pi K_E d_p \bar{c}_i e^2 N_i t}{2kT}\right) \tag{3.44}$$

where d_p is the particle diameter, k is the Boltzmann's constant, $K_E = 1/4\pi\varepsilon_0 = 9.0\times10^9$, $\bar{c}_i$ is the mean thermal speed of the ions, and T is the operating temperature. For the field charge, n_{field}, can be calculated by the field charging equation derived by Panthenier and Moreau-Hanot (1932) and White (1951), is given by

$$n_{\mathrm{field}} = \left(1 + 2\frac{\varepsilon - 1}{\varepsilon + 2}\right)\left(\frac{Ed_p^2}{4K_E e}\right)\left(\frac{\pi K_E e Z_i N_i t}{1 + \pi K_E e Z_i N_i t}\right) \tag{3.45}$$

where ε is the dielectric constant of particle, and E is the average electric field strength in the charging region of the charger. Finally, both field and diffusion charging occur at the same time. This is known as continuum charging where particle charge is the sum of the contributions from field and diffusion charging (Liu and Kapadia 1978). For the particle diameter less than 1 μm, the electric field that existed in the charger should have a negligible effect on the charging process (Pui 1976).

(d) Estimation of the penetration through the charger

The particle loss inside the charger due to the electrostatic loss is defined as the ratio of the charged particles concentration at the outlet over the total concentration of uncharged particle at the inlet of the charger. The particle penetration, P, through the charger can be calculated by Deutsch-Anderson equation as (Hinds 1999)

$$P = \exp\left(-\frac{2Z_p E(r) t}{r}\right) \tag{3.46}$$

where Z_p is the electrical mobility of particle, $E(r)$ is the electric field strength in the charging region as a function of radial distance, t is the mean residence time, and r is the outer electrode radius. In this study, the particle loss inside the charger is primarily due to the strong electric field caused by the corona discharge. Diffusion and gravitational losses are not significant.

3.2.3 Numerical Models

A numerical model was developed to investigate flow and electric fields in the charging zone of the charger to give a better understanding on the operating of both chargers. The model is consists of two parts; flow field and electric field modeling. For flow field modeling, flow conditions inside the charger are assumed to be steady, incompressible and laminar. Based on the principle of momentum conservation, the continuity and the incompressible Navier-Stokes equations (N-S equation) in the 2-D cylindrical coordinates can be used in this model. For the boundary conditions used, no slip boundary is applied to all the solid walls included in the computation domain, and fixed velocity boundary condition was applied to the aerosol inlet. The velocity at inlet was calculated from the flow rate through the charger. Uniform velocity profile is assumed at the aerosol inlet across the cross section of the inlet tubes. For electrostatic field modeling, the Poisson's equation for the electric potential can be used in this case. For the boundary conditions used, constant potentials are applied to the corona-electrode (V = corona voltage), the outer electrode ($V = 0$), and the zero gradient conditions is applied to the boundaries with out walls. For the complex geometry, the continuity and the N-S equation (Equation 2.47 – 2.50) for flow field and the Laplace's equation (Equation 2.52) for the electric potential were numerically solved using a commercial computational fluid dynamic software package, CFDRC™. The CFDRC™ package adopts finite-volume method (CFDRC Manual 2000). The solution domain is divided into a number of cells known as control volumes. In the finite volume approach of CFDRC™, the governing equations are numerically integrated over each of these computational cells or control volumes. Figure 3.7 shows computational domains in the charging zone for each charger. Figure 3.8 shows a cross-section of the computational mesh distribution used for the flow and electric field simulations for each charger. A structured grid is used. A total of about 6,000 meshes are distributed in computational domain of the corona-needle charger (Figure 3.8.a.), while the corona-wire charger, a mesh with about 4000 meshes is used (Figure 3.8.b.).

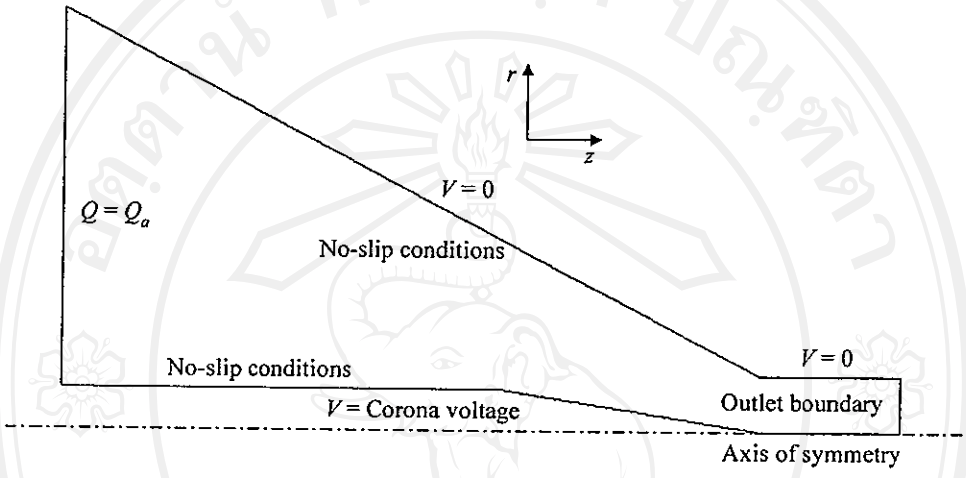

(a) needle

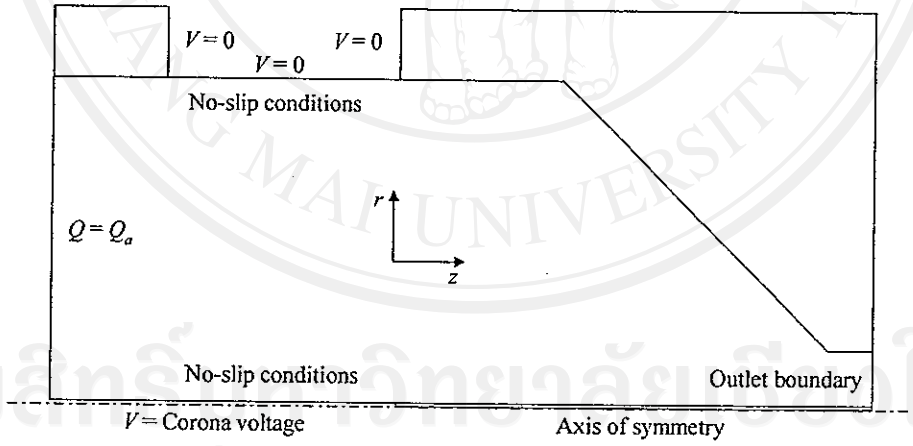

(b) wire-cylinder

Figure 3.7 Computational domains of the corona-needle and wire chargers.

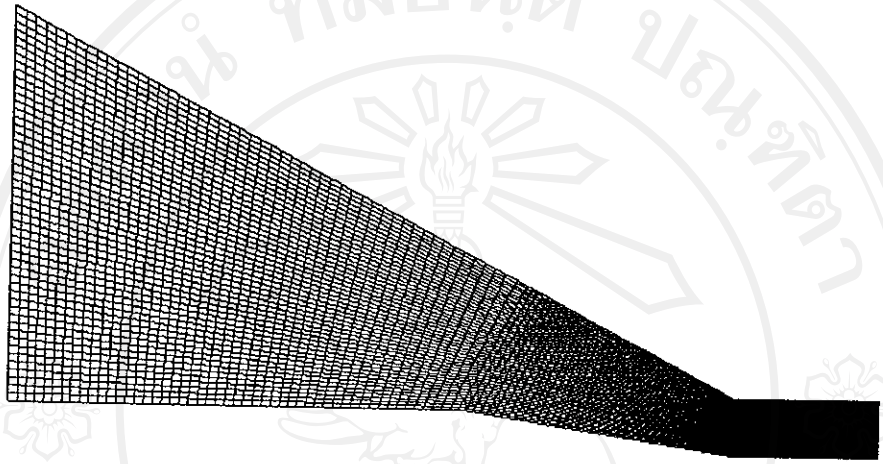

(a) needle

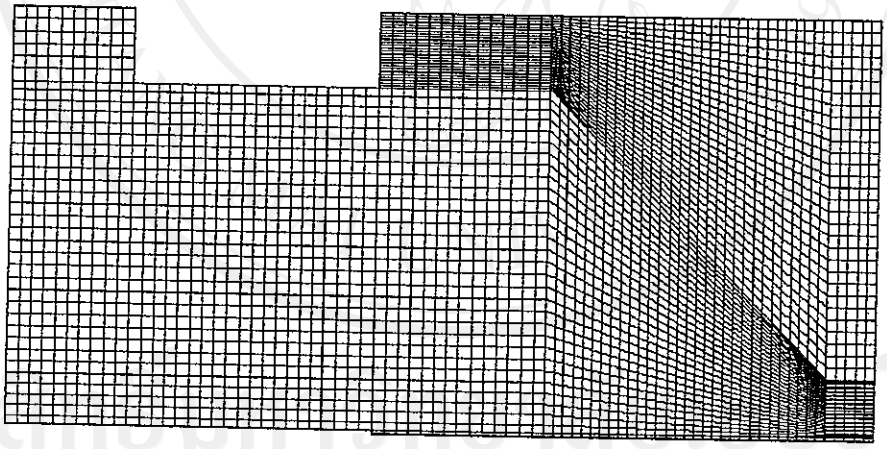

(b) wire-cylinder

Figure 3.8 Computational mesh distributions for the corona-needle and wire chargers.

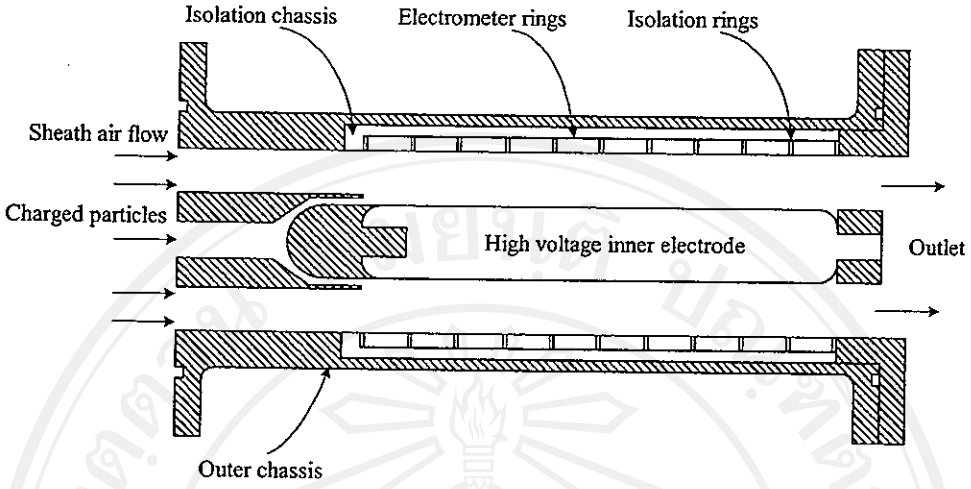

Figure 3.9 Schematic diagram of the mobility classifier.

3.3 Mobility Classifier

3.3.1 Description

The mobility classifier has one short column which consists of coaxially cylindrical electrodes. A schematic diagram of the mobility classifier used in this thesis study is depicted in Figure 3.9 (detailed drawings are provided in Appendix A.4). Its geometrical configuration is similar to the classifier used by Graskow (2001), Reavell *et al.* (2001), and Biskos (2004). The outer chassis is made of a stainless steel tube a 50 mm in diameter and the inner electrode is made of aluminum rod a 20 mm in diameter and 131 mm in length. The inner electrode was polished to an extremely fine surface finish to avoid undesirable electric field effect on particle motion due to non-uniform electric field which results from small surface scratches and imperfections. Both ends of the inner electrode were rounded to a 5 mm radius to avoid distortion of the electric field which would result from sharp edges. The advantage of cylindrical geometry is that distortion of electric field between electrodes is minimal due to the absence of corners and edges. Operation and performance of the instrument depend upon aerosol transport under the influence of flow and electric fields. It was important to ensure that both flow and electric fields were laminar and uniformly distributed inside the classifying column. There are two streams which are the aerosol and sheath air flows. Inner walls of flow paths and curvature at the transition into the classifying section were designed such that smooth and turbulence free merging of the two gases flows are provided. The inner electrode of the classifier is maintained at a positive high voltage while the outer chassis of the classifier is grounded. An adjustable DC high voltage power supply is used to maintain this voltage difference, generally in the range between 500 V – 3.0 kV. It should be noted that the applied high voltage is maintained at a lower value than the corona onset voltage to avoid unintentional charging of the particles within the classifier. The charged particles enter the classifier column close to the inner electrode by a continuous flow of air, and surrounded by a sheath air flow. Since the inner electrode is kept at a positive high voltage, the charged particles are deflected outward radially. They are collected on a series of ten electrically isolated electrometer rings positioned at the inner surface of the outer electrode of the column. Electrometers connected to these electrometer rings measure currents corresponding to the number concentration of particles of a given mobility which is related to the particle size. Resolution and size range of the whole instrument is determined mainly by the number and width of the electrometer rings.

Table 3.1 Electrometer ring width and positions along the size classification column.

Electrometer Ring Number	Electrometer Ring Width (mm)	Midpoint Location (mm)
1	12	7
2	12	20
3	12	33
4	12	46
5	12	59
6	12	72
7	12	85
8	12	98
9	12	111
10	12	124

Table 3.1 shows the width and the position of the electrometer rings along the mobility classification column. The 10 electrometer rings used result in the classification of every measured aerosol into 10 mobility ranges. As shown in Table 3.1, the electrometer rings have a width of 12 mm. The first electrometer ring is located 1 mm downstream the aerosol inlet, while a 1.0 mm gap is allowed between the electrometer rings for isolation. Electrical current detection method was considered to be easier and faster than direct particle detection measurements. The size range and resolution of particle collected on the electrometer rings can be also varied by adjusting the sheath air and aerosol flow rates, the voltage applied to the inner electrode, and the operating pressure. Figure 3.10 shows a picture of the mobility classifier.

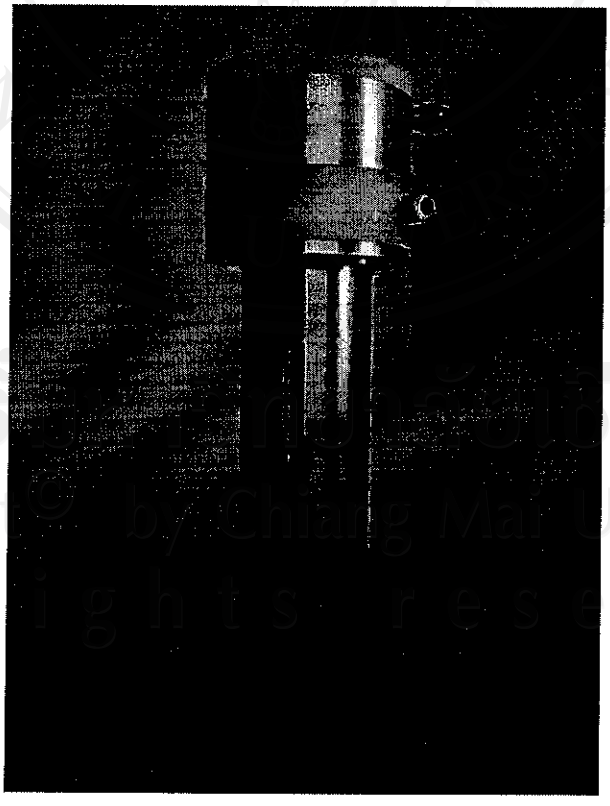

Figure 3.10 A picture of the mobility classifier column.

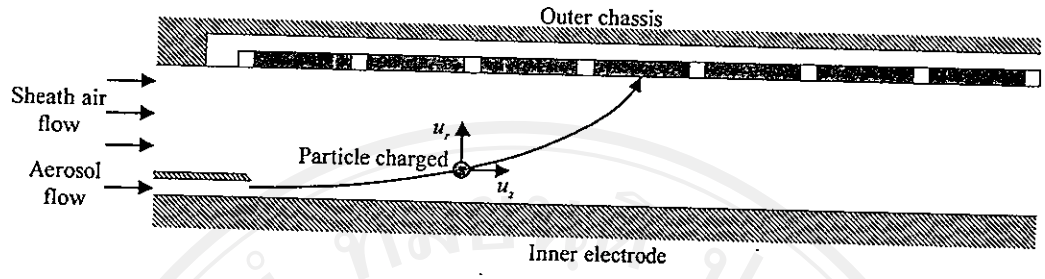

Figure 3.11 Schematic diagram of non-diffusing particle trajectory in the mobility classifier.

3.3.2 Analytical Models

In this Section, there are two approaches were used to predict the performance of the classifier column. The first one is an analytic solution of the equations that describe motion of charged particles in electric field was used to predict the landing location of particles along the classification column with and without Brownian diffusion effect, while the second is the expression for the prediction of the mobility and size classification of the classifier column.

(a) Non-Diffusing Particle Trajectory

In this Section, rather than the transfer function method, the particle trajectory method was employed. How charged particles are influenced by an electric field, perpendicular to the particles initial trajectory, are also described in this Section. Design of the electrical mobility classifiers ranging from simple parallel-plate to more complicated radial geometries have been proposed and used successfully. However, the most common electrical mobility classifiers employ annular configurations where the axially moving sample is exposed to a radial electric field. Figure 3.11 shows a schematic diagram of a non-diffusing particle trajectory in the mobility classifier. The axial motion was influenced by the fluid velocity profile in the axial flow. The radial motion is due to electric force which is by far greater than other forces. When the particles introduced into the classification column, any charged particle under the influence of an electric field will have an electrical mobility. It is assumed that:

1. The flow and electric fields are axisymmetric and steady,
2. The flow in the classifier is laminar, fully developed and incompressible ($\nabla \cdot u = 0$),
3. The space charge effect is negligible ($\nabla \cdot E = 0$), and
4. Gravitational and Brownian diffusion effects are negligible.

The total volumetric flow rate, Q_t, through the classifier column is

$$Q_t = Q_{sh} + Q_a \tag{3.47}$$

where Q_{sh} is the particle free sheath air flow rate and Q_a is the aerosol flow rate. For the particular case of annular geometries where the charged aerosol sample enters the classifier on an axial flow and the charged particles migrate along the radial direction of electric field, motion of the charged particles within the classification column can be described by the system of differential equations as (Knutson and Whitby 1975)

$$\frac{dr}{dt} = u_r + Z_p E_r \tag{3.48}$$

$$\frac{dz}{dt} = u_z + Z_p E_z \tag{3.49}$$

where r and z are the radial and axial dimensions of the classifier, u_r and u_z are the radial and axial components of the air flow velocity. Similarly, E_r and E_z are the radial and axial components of the electric field and Z_p is the electrical mobility of particles. When a uniform electric field is established between the two electrodes of the classifier, the electric field components are given by the following relations

$$E_r = \frac{V}{r \ln(r_2/r_1)} \quad \text{and} \quad E_z \approx 0 \tag{3.50}$$

where r_1 and r_2 are the radii of the inner and outer electrodes respectively. Assuming that the radial velocity component for a laminar annular flow is zero (u_r = 0) and combining the above equations, the charged particle trajectories in a plug flow can be described by

$$\frac{dr}{dt} = \frac{Z_p V}{r \ln(r_2/r_1)} \tag{3.51}$$

$$\frac{dz}{dt} = u_z \tag{3.52}$$

Using Equations 3.51 and 3.52, the trajectory of the charged particle is given by

$$\frac{dr}{dz} = \frac{\frac{dr}{dt}}{\frac{dz}{dt}} = \frac{Z_p V}{r u_z \ln(r_2/r_1)} \tag{3.53}$$

Integrating Equation 3.53, the migration paths of the charged particles can be determined as

$$\int_{r_{in}}^{r_2} r u_z dr = \int_0^z \frac{V Z_p}{\ln(r_2/r_1)} dz \tag{3.54}$$

where r_{in} is the radial position at which the particle enters the classifier. Assuming that the average flow velocity in the axial direction of the classifier column is

$$u_z = \frac{Q_t}{\pi(r_2^2 - r_1^2)} \tag{3.55}$$

Therefore, the deposition of the charged particles entering the classifier column at a radial position of r_{in} has trajectory taking it to an axial position z downstream the aerosol inlet is given in terms of their electrical mobility, the mean flow velocity, and the electric field strength is

$$z = \frac{Q_t \ln(r_2/r_1)\left(r_2^2 - r_{in}^2\right)}{2\pi V Z_p \left(r_2^2 - r_1^2\right)} \tag{3.56}$$

which rearranges in terms of the critical electrical mobility of a particle that is collected on the outer electrode at distance z downstream the aerosol inlet can be calculated as

$$Z_p = \frac{Q_t \ln(r_2/r_1)\left(r_2^2 - r_{in}^2\right)}{2\pi V z \left(r_2^2 - r_1^2\right)} \tag{3.57}$$

For viscous flow, $u_r \approx 0$, $u_z = u_z(r)$, $E_r(r) = V/r \ln(r_2/r_1)$, and $E_z = 0$. Substituting into Equations 3.48 and 3.49 gives the following differential equations describing the trajectory of an aerosol particle in a viscous flow (Hagwood *et al.* 1999):

$$\frac{dr}{dt} = \frac{Z_p V}{r \ln(r_2/r_1)} \tag{3.58}$$

$$\frac{dz}{dt} = u_z(r) = Ar^2 + B\ln(r) + C \tag{3.59}$$

where:

$$A = \frac{1}{4\mu}\frac{dp}{dz},\quad B = -\frac{1}{4\mu}\frac{dp}{dz}\left(\frac{r_2^2 - r_1^2}{\ln(r_2/r_1)}\right),\quad C = \frac{1}{4\mu}\frac{dp}{dz}\left(\frac{r_2^2 - r_1^2}{\ln(r_2/r_1)}\ln(r_1) - r_1^2\right),$$

dp/dz denotes the constant pressure gradient is given by the following equations

$$\frac{dp}{dz} = -\frac{\rho \bar{U}^2 f}{2D_h} \tag{3.60}$$

where:

$$D_h = 2r_2\left(1 - (r_1/r_2)\right), \tag{3.61}$$

$$f = \frac{64}{\mathrm{Re}}\left(\frac{1 + (r_1/r_2)^2}{\left(1 - (r_1/r_2)\right)^2} + \frac{1 + (r_1/r_2)}{\left(1 - (r_1/r_2)\right)\ln(r_1/r_2)}\right)^{-1}, \tag{3.62}$$

$$\mathrm{Re} = \frac{2r_2\left(1 - (r_1/r_2)\right)\bar{U}\rho}{\mu}, \tag{3.63}$$

D_h is the hydraulic diameter for an annular flow area, f is the friction factor, $\bar{U}$ is the mean axial flow velocity, ρ is the gas density and Re is the Reynolds number in the annular flow.

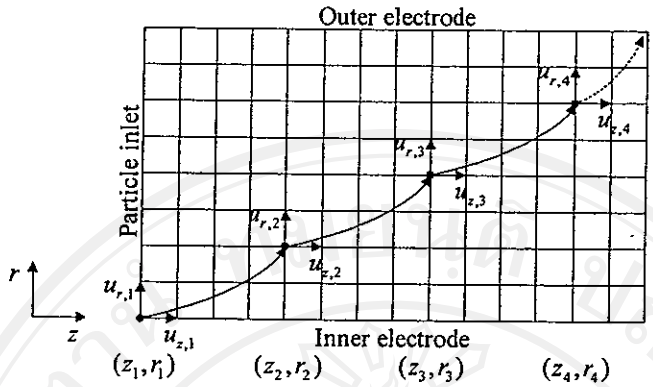

Figure 3.12 Non-diffusing particle trajectory model.

Using Equations 3.58 and 3.59, the trajectory of the charged particle in a viscous flow is given by

$$\frac{dr}{dz} = \frac{\frac{dr}{dt}}{\frac{dz}{dt}} = \frac{Z_p V}{r u_z(r) \ln(r_2/r_1)} \tag{3.64}$$

Integrating Equation 3.64, the migration paths of the charged particles can be determined. Their landing location downstream of the aerosol inlet is given in terms of their electrical mobility, the flow velocity profile, and the electric field strength:

$$\int_{r_{in}}^{r_2} r u_z(r) dr = \int_0^z \frac{V Z_p}{\ln(r_2/r_1)} dz \tag{3.65}$$

The particle entering the classifier at a radial position of r_{in} has trajectory taking it to an axial position of z, which can be obtained as

$$z = -\frac{\ln(r_2/r_1)}{4VZ_p}\begin{pmatrix} Ar_2^4 - Ar_{in}^4 + Br_{in}^2 - Br_2^2 + 2Br_2^2 \ln(r_2) \\ -2Br_{in}^2 \ln(r_{in}) + 2Cr_2^2 - 2Cr_{in}^2 \end{pmatrix} \tag{3.66}$$

and the expression for the trajectory of the particle with viscous flow entering the spectrometer at a radial position of $r_{in} + \delta$ which has trajectory taking it to an axial position of z and is given by

$$z = -\frac{\ln(r_2/r_1)}{4VZ_p}\begin{pmatrix} Ar_2^4 - Ar_{in}^4 - A\delta^4 - 4A\delta^3 r_{in} - 4A\delta r_{in}^3 - 6A\delta^2 r_{in}^2 \\ +Br_{in}^2 - Br_2^2 + B\delta^2 + 2B\delta r_{in} + 2Br_2^2 \ln(r_2) \\ -2Br_{in}^2 \ln(r_{in} + \delta) - 2B\delta^2 \ln(r_{in} + \delta) \\ -4B\delta r_{in} \ln(r_{in} + \delta) + 2Cr_2^2 - 2Cr_{in}^2 - 2C\delta^2 - 4C\delta r_{in} \end{pmatrix} \tag{3.67}$$

Figure 3.12 shows a computational model used for the particle trajectory simulation. The radial and axial positions of particle trajectories can be calculated using Equation 3.66 and 3.67. By knowing the initial position and calculating the radial and axial displacements of

particles, their new positions within the classification column were evaluated. These calculations are repeated until the particles reach the boundaries of the solution model (outer electrode). Once, the particle trajectories inside the classifier are known, size classification of deposited particles can be determined.

(b) Diffusing Particle Trajectory

As a result of random collisions between the aerosol particles and the air molecules, aerosol particles undergo diffusion. Diffusion is reflected in the aerosol particle's trajectory as a random perturbation. These perturbations are described by Brownian motion. The behavior of nanometer-sized particles in the size classifier can be described by the convective Brownian diffusion equation (Kousaka *et al.* 1986)

$$u(r)\frac{\partial n(r,z)}{\partial r} = D\left(\frac{\partial^2 n(r,z)}{\partial r^2} + \frac{1}{r}\frac{\partial n(r,z)}{\partial r} + \frac{\partial^2 n(r,z)}{\partial z^2}\right) - \frac{1}{r}\frac{\partial}{\partial r}\left(Z_p r E(r) n(r,z)\right), \qquad (3.68)$$

where r and z are the radial and axial positions, $u(r)$ is the axial velocity of gas flow, n is the particle number concentration, and D is the Brownian diffusion coefficient. Equation 3.68 can be normalized using three dimensionless parameters as (Kousaka *et al.* 1986)

$$\overline{u}(\overline{r}) = \frac{u(r)}{u_{av}}, \qquad (3.69)$$

$$\overline{D} = \frac{Dz}{r_1^2 u_{av}}, \qquad (3.70)$$

$$\overline{E} = \frac{Z_p V z}{r_1^2 u_{av} \ln\left(r_2/r_1\right)}, \qquad (3.71)$$

where $\overline{u}$, $\overline{D}$, and $\overline{E}$ are the normalized gas velocity, diffusivity, and velocity due to electrostatic force, respectively, Z_p is the electrical mobility of particle, z is the axial distance, V is the applied voltage, u_{av} is the average gas flow velocity in the classifier, r_1 is the inner electrode and r_2 is outer electrode. The value of $\overline{D}/\overline{E}$ is important in the evaluation of the effect of Brownian diffusion. In the ideal case with on Brownian diffusion motion, the value of $\overline{D}/\overline{E}$ becomes zero (Kousaka *et al.* 1986). Brownian motion also causes particles to deviate from their ideal transport paths within the classifier column resulting in a diffusion broadening of the mobility range collected on the electrometer ring as shown in Figure 3.13. In ideal particle motion (no diffusion), the radial position of the velocity of particle is given by

$$\frac{dr}{dt} = \frac{VZ_p}{r\ln\left(r_2/r_1\right)} \qquad (3.72)$$

where r is the radial distance, and V is the applied voltage. In Brownian diffusion motion, a particle of mobility Z_p arrives at each electrometer ring at a radial position given by a certain probability distribution, which is assumed to be a Gaussian of mean r and standard deviation σ_{diff}.

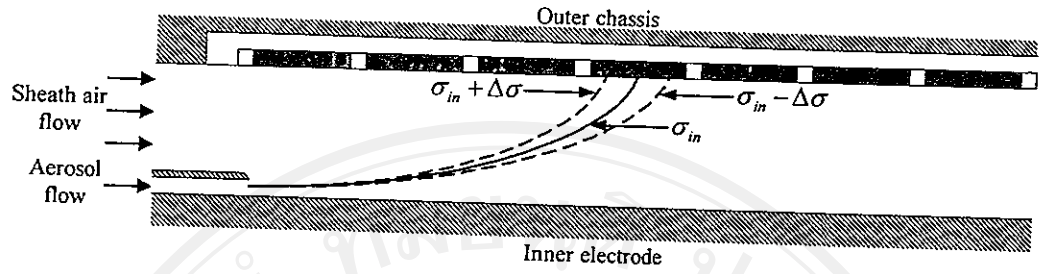

Figure 3.13 Schematic diagram of diffusing particle trajectory in the mobility classifier.

The mean value of the trajectory end-point distribution is determined by the applied electric field

$$r(t)=\sqrt{r_0^2+\frac{2Vt}{\ln(r_2/r_1)}Z_p} \tag{3.73}$$

where r_0 is the initial radial position of the particle at time $t = 0$, and t is the mean aerosol residence time between the inlet and electrometer rings. The variance of the trajectory end-point distribution is assumed to be that of a pure Brownian process, and given by

$$\sigma_{\text{diff}} \approx \sqrt{2Dt}, \tag{3.74}$$

where:

$$D=\frac{kTZ_p}{ne} \tag{3.75}$$

is the particle diffusion coefficient which is a function of the electrical mobility of particle. The radial position of particles r_{diff} takes into account the Brownian diffusion motion. A particle which enters the classifier at position r_0 and arrives at electrometer ring at a position $r \pm \sigma_{\text{diff}}$ is given by

$$r_{\text{diff}} = r \pm \sigma_{\text{diff}} \tag{3.76}$$

where r is the radial distance, and σ_{diff} is the standard deviation of the trajectory end-point distribution for particles. The plus sign indicates that the upper limit of the diffusive particle trajectory. The minus sign indicates that the lower limit of the diffusive particle trajectory. Inserting Equations 3.73 and 3.74 into Equation 3.76 leads to the radial position for diffusive particles is given by

$$r_{\text{diff}}(t)=\sqrt{r_0^2+\frac{2VZ_pt}{\ln(r_2/r_1)}\pm\frac{2kTZ_pt}{ne}} \tag{3.77}$$

Substituting $t = z/u_{av}$ into Equation 3.77, the diffusive particle trajectory is

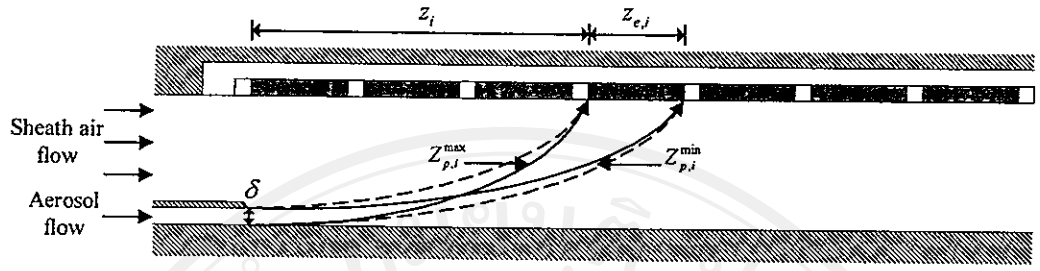

Figure 3.14 Principle of the mobility and size classification in the classifier.

$$r_{diff}(z) = \sqrt{r_0^2 + \frac{2VZ_p z}{u_{av}\ln(r_2/r_1)} \pm \frac{2kTZ_p z}{u_{av} ne}} \tag{3.78}$$

With the Equation 3.78, the above equation can now be solved explicitly for the diffusive particle trajectory. The maximum relative error committed when using this approximation is only 2.3% (Alonso and Kousaka 1996).

(c) Mobility and Size Classification

The theoretical background on particle trajectory previously described was used in designing the spectrometer. Although this information is important for the analysis of the classifier, it is not sufficient to describe its overall performance. A more complete description of classification process is provided by the mobility and size classification which gives the window of particle mobilities collected on every electrometer ring. In order to classify particle size, the particle electrical mobility was considered. The design practice was similar to Mirme (1994), Tammet *et al.* (2001), Graskow (2001), Kulon *et al.* (2001), and Biskos (2004). The classifier column was divided into a number of well-insulated virtual ground electrometer rings ($R > 10^{12}$ Ω). Figure 3.14 shows the principle of the mobility and size classification. Each outer electrometer ring of the spectrometer represents one size classification channel and its axial location along the column depends on the particle electrical mobility. When the Brownian diffusion motion of the particle is not significant, considering one particular electrometer ring; the particle enters the spectrometer at the position immediately adjacent to the inner wall (at $r_{in} = r_1$), and is deposited at the leading edge of the ring (at $z = z_i$). In this case, the maximum mobility, $Z_{p,i}^{max}$, of particle to deposit on this ring is

$$Z_{p,i}^{max} = -\frac{\ln(r_2 - r_1)}{4Vz_i}\begin{pmatrix} Ar_2^4 - Ar_1^4 + Br_1^2 - Br_2^2 + 2Br_2^2\ln(r_2) \\ -2Br_1^2\ln(r_1) + 2Cr_2^2 - 2Cr_1^2 \end{pmatrix} \tag{3.79}$$

where z_i is the axial position between the aerosol entry location and the leading edge of the electrometer ring. This equation can be used to determine the diameter of the particle where all the terms are known. Using Stoke's law to classically define the electric mobility, Z_p which can be written in terms of $d_{p,i}^{max}$, the particle diameter with the maximum mobility is given by

$$d_{p,i}^{\max} = -\frac{4Vz_i n(d_{p,i}^{\max}) e C_c(d_{p,i}^{\max})}{3\pi\mu \ln(r_2/r_1)} \begin{pmatrix} Ar_2^4 - Ar_1^4 + Br_1^2 - Br_2^2 + 2Br_2^2 \ln(r_2) \\ -2Br_1^2 \ln(r_1) + 2Cr_2^2 - 2Cr_1^2 \end{pmatrix}^{-1} \tag{3.80}$$

Similarly, the minimum mobility, $Z_{p,i}^{\min}$, of the particle that enters the spectrometer at the outer most radial position of the aerosol inlet (at $r_{in} = r_1 + \delta$) and deposits at the trailing edge of the ring (at $z = z_i + z_{e,i}$) is

$$Z_{p,i}^{\min} = -\frac{\ln(r_2/r_1)}{4V(z_i + z_{e,i})} \begin{pmatrix} Ar_2^4 - Ar_1^4 - A\delta^4 - 4A\delta^3 r_1 - 4A\delta r_1^3 - 6A\delta^2 r_1^2 \\ +Br_1^2 - Br_2^2 + B\delta^2 + 2B\delta r_1 + 2Br_2^2 \ln(r_2) \\ -2Br_1^2 \ln(r_1 + \delta) - 2B\delta^2 \ln(r_1 + \delta) \\ -4B\delta r_1 \ln(r_1 + \delta) + 2Cr_2^2 - 2Cr_1^2 - 2C\delta^2 - 4C\delta r_1 \end{pmatrix} \tag{3.81}$$

where $z_{e,i}$ is the width of the electrometer ring, and δ is the width of the aerosol flow inlet. The particle size, $d_{p,i}^{\min}$, with the minimum mobility is given by

$$d_{p,i}^{\min} = -\frac{4V(z_i + z_{e,i}) n(d_{p,i}^{\min}) e C_c(d_{p,i}^{\min})}{3\pi\mu \ln(r_2/r_1)} \times \begin{pmatrix} Ar_2^4 - Ar_1^4 - A\delta^4 - 4A\delta^3 r_1 - 4A\delta r_1^3 - 6A\delta^2 r_1^2 + Br_1^2 - Br_2^2 \\ +B\delta^2 + 2B\delta r_1 + 2Br_2^2 \ln(r_2) - 2Br_1^2 \ln(r_1 + \delta) - 2B\delta^2 \ln(r_1 + \delta) \\ -4B\delta r_1 \ln(r_1 + \delta) + 2Cr_2^2 - 2Cr_1^2 - 2C\delta^2 - 4C\delta r_1 \end{pmatrix}^{-1} \tag{3.82}$$

Only particles with electrical mobility between these two limits $Z_{p,i}^{\min} < Z_{p,i} < Z_{p,i}^{\max}$ will deposit on this electrometer ring and contribute to the measured signal current. The range of electrical mobility is a function of the voltage applied to the central rod electrode, flow settings and geometrical factors of the classifier column.

It can be seen that Equation 3.80 and 3.82 defines the diameter of a particle, d_p, for a given voltage and classifier column geometry. However, there are two variables on the right hand side of these Equation (namely the number of charges on the particle, n, and the Cunningham slip correction factor, C_c) are function of the particle diameter. Therefore, an iterative method is needed to calculate the value of the particle diameter. In this study, the Secant's iteration was used. The Secant's method is obtained from Newton's method by approximating the derivative of function $F(x)$ at two points x_n and x_{n-1} is given by

$$x_{n+1} = x_n - \frac{F(x_n)}{F'(x_n)}, \tag{3.83}$$

where:

$$F'(x_n) = \frac{F(x_n) - F(x_{n-1})}{(x_n - x_{n-1})} \tag{3.84}$$

Substituting into Equation 3.83 gives

$$x_{n+1} = x_n - \frac{F(x_n)(x_n - x_{n-1})}{F(x_n) - F(x_{n-1})} \tag{3.85}$$

By iteration, this approximation should converge to a single value. The function used in the iteration to calculate the particle diameter is $V(d_p)$, the voltage function and is defined as:

$$V(d_p) = V_0 - \left(X \frac{d_p}{n(d_p) C_c(d_p)} \right), \tag{3.86}$$

where:

$$X = -\frac{3\pi\mu \ln(r_2/r_1)}{4ez_i} \begin{pmatrix} Ar_2^4 - Ar_1^4 + Br_1^2 - Br_2^2 + 2Br_2^2 \ln(r_2) \\ -2Br_1^2 \ln(r_1) + 2Cr_2^2 - 2Cr_1^2 \end{pmatrix}, \quad \text{for } d_p^{\max} \tag{3.87}$$

$$X = -\frac{3\pi\mu \ln(r_2/r_1)}{4e(z_i + z_{e,i})} \begin{pmatrix} Ar_2^4 - Ar_1^4 - A\delta^4 - 4A\delta^3 r_1 - 4A\delta r_1^3 \\ -6A\delta^2 r_1^2 + Br_1^2 - Br_2^2 + B\delta^2 + 2B\delta r_1 \\ +2Br_2^2 \ln(r_2) - 2Br_1^2 \ln(r_1 + \delta) \\ -2B\delta^2 \ln(r_1 + \delta) - 4B\delta r_1 \ln(r_1 + \delta) \\ +2Cr_2^2 - 2Cr_1^2 - 2C\delta^2 - 4C\delta r_1 \end{pmatrix}, \quad \text{for } d_p^{\min} \tag{3.88}$$

V_0 is the actual voltage of the inner electrode. Substituting Equation 3.86 into Equation 3.85, and replacing x_{n-1} with d_{p1} and x_n with d_{p0} gives:

$$d_{p1} = d_{p0} - \frac{V(d_{p0})(d_{p0} - d_{p1})}{V(d_{p0}) - V(d_{p1})} \tag{3.89}$$

or

$$d_{p1} = d_{p0} - \frac{(d_{p0} - d_{p1}) \left(V_0 - \left(X \frac{d_{p0}}{n(d_{p0}) C_c(d_{p0})} \right) \right)}{X \left(\frac{d_{p1}}{n(d_{p1}) C_c(d_{p1})} - \frac{d_{p0}}{n(d_{p0}) C_c(d_{p0})} \right)} \tag{3.90}$$

The process is repeated, each time with the new approximation for the particle diameter, d_{p1}. Then the current value of d_{p1} is outputted as the diameter of charged particle that was measured from each electrometer ring for the given voltage and classifier column geometry.

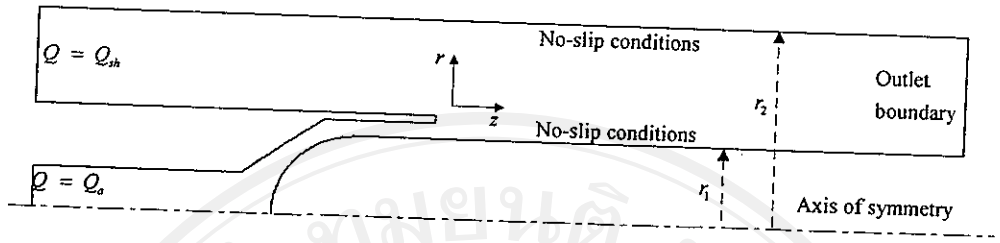

Figure 3.15 Computational domain for flow field calculation.

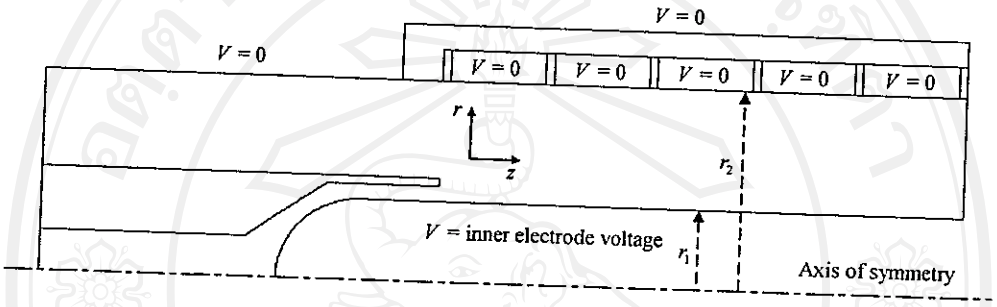

Figure 3.16 Computational domain for electric field calculation.

3.3.3 Numerical Models

In addition to the analytical theory described above, a numerical model was developed to investigate flow and electric fields inside the classifier column to given a better understanding on the operation of the EMS. The proposed model consists of two parts, flow field and electric field modeling. The assumptions involved is presented in the following sections. Flow condition in the classifier is designed to be in the laminar regime. Turbulent mixing which can deteriorate the classifier performance should be avoided. However, depending on the flow conditions of sheath air and aerosol inlet, the flow may become turbulent. Further, the classifier is operated at fixed (steady) and low Mach number (incompressible) flow rates for most applications. Under these conditions, the flow inside the instrument can be assumed to be steady, incompressible and laminar. Based on the principle of momentum conservation, the incompressible N-S equations can be applied in this case. The continuity and N-S equations in 2-D cylindrical coordinates can be used in this model. For the boundary conditions used, no slip boundary is applied to all the solid walls included in the computation domain and fixed velocity boundary conditions were applied to the aerosol and sheath air flow inlets as shown in Figure 3.15. The velocities at each inlet were calculated from the flow rates through these slits. Uniform velocity profile is assumed at the sheath and aerosol inlet across the cross section of the inlet tubes. For electric field modeling, the Laplace's equation for the electric potential can be used in this case. For the boundary conditions used, constant potentials are applied to the inner electrode (V = inner electrode voltage), the outer chassis ($V = 0$), and at each electrometer ring ($V = 0$) and the zero gradient conditions is applied to the boundaries without walls as shown in Figure 3.16. The continuity and the N-S equation (Equation 2.47 – 2.50) for flow and the Laplace's equation (Equation 2.52) for electric potential cannot be solved analytically in this study, especially for the complex geometry of aerosol flow path and instrumental design. Numerical approach has to be performed in order to obtain the solutions. The commercial computational fluid dynamic software package, CFDRC™ is employed in this study.

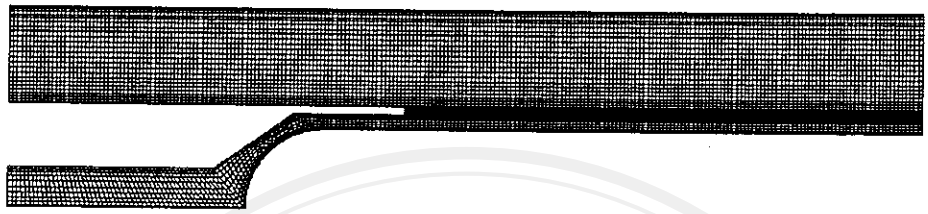

Figure 3.17 Mesh distribution for flow field calculation.

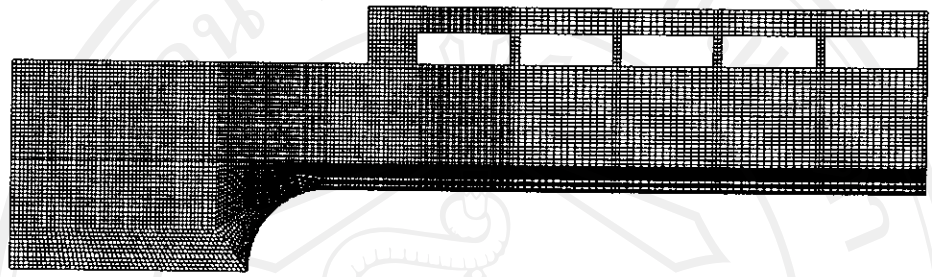

(a)

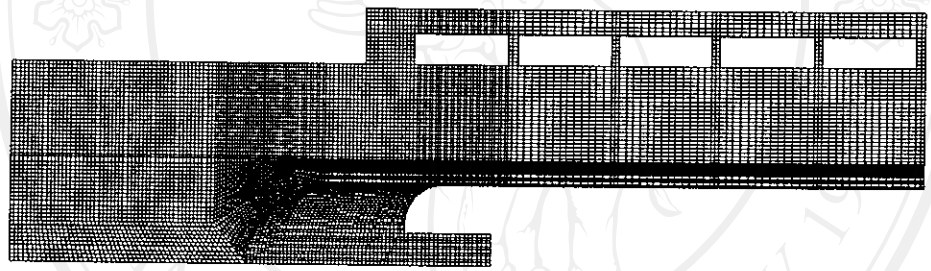

(b)

Figure 3.18 Mesh distribution for electric field calculation

Figure 3.17 shows a cross-section of the mesh distribution used for the flow field simulations. Finer grids are used in the region close to the aerosol entrance and where the velocity gradient is expected to be large. A structured mesh is used. A total of about 10,232 meshes are distributed in computational domain of internal flows in the classifier. Figure 3.18 shows a cross-section of the mesh distribution used for the electric field simulations for case (a) with inlet flow guide made of conductor and (b) with inlet flow guide made of insulator. In this computational domain of electric field in a classifier, a mesh with about 12,000 cells is used.

3.4 Electrometer

3.4.1 Description

Figure 3.19 shows the electrometer circuit design used to amplify the signal current from the electrometer rings of the classifier column. This circuit consists of simple current to voltage converters, where the voltage drop caused by a current flowing through a resistor is measured. The circuit which was constructed used the two cascaded negative feedback amplifier (the extra components in this circuit are primarily for fine offset voltage adjustment and input/output protection).

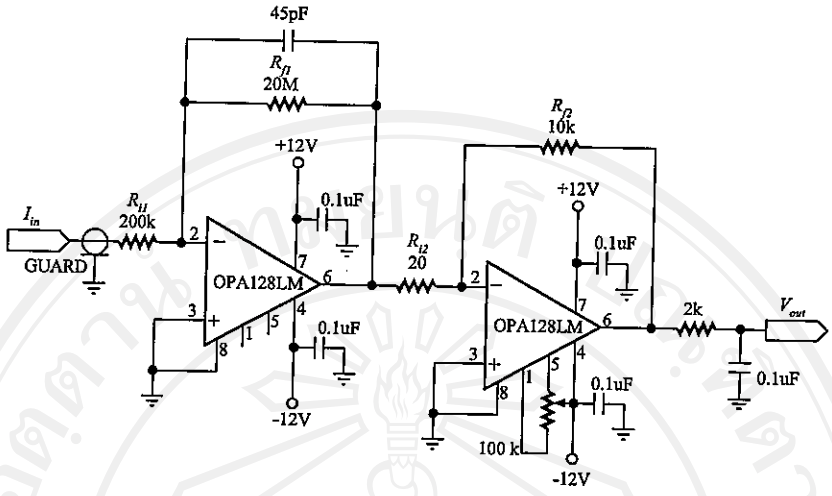

Figure 3.19 Schematic diagram of the electrometer circuit design.

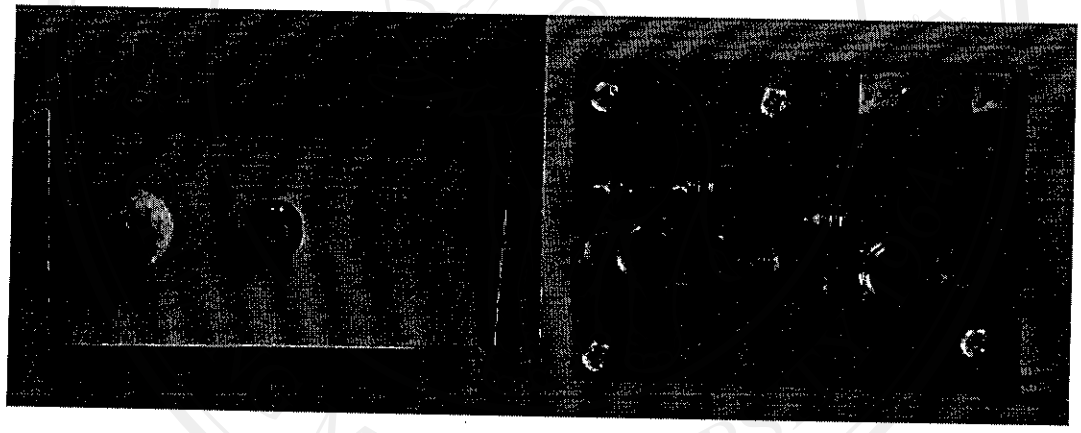

Figure 3.20 A picture of the electrometer circuit.

The feedback capacitor and RC low-pass filter shown in Figure 3.19 are used to reduce high frequency noise and to prevent oscillations of the amplifier output. In order to avoid expensive construction due to the need for multiple electrometers, low-cost monolithic operation amplifiers are used. The amplifier used in this circuit is the Burr-Brown OPA128LM (improved replacement for AD515 and AD549), which is design for low current measurement and features ultralow input bias current (> 75 fA maximum) and low induced input noise (> 4 μV peak-to-peak). Figure 3.20 shows a picture of the electrometer circuit. While the design of the electrometer circuit is relatively simple, construction of the circuits is somewhat less straightforward. Because of the extremely low current levels being measured, standard circuit fabrication techniques are not satisfactory. The reason for this is that stray leakage currents between the circuit power supply and the electrometer inputs (through the printed circuit board material itself) are more than sufficient to overwhelm the measured input currents. In addition, the presence of any oils or other contaminants from fingerprints or anti-static treatment chemicals may provide conductive path with lower resistance than the intended circuit paths. To avoid leakage problems, the amplifier inputs are all isolated from the printed circuit board: connection pins are held against the electrometer ring using Teflon standoffs, and connections between these pins and the amplifier inputs are made in air, above the circuit board.

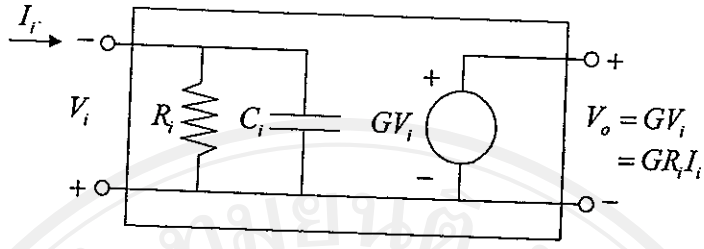

Figure 3.21 Two-port model of the electrometer circuit.

Contamination is minimized first by cautious fabrication techniques, and secondly by thorough cleaning of the assembled circuit (ultrasonic bath followed by rinsing in isopropyl alcohol) following fabrication. Further references on low-current circuit fabrication techniques can be found in (AD549; OPA128; Pease 1993; Graskow 2001).

3.4.2 Analytical Model

In this Section gives the analytical model of the electrometer circuit design (Figure 3.19). The electrometer circuit is simply a shunt resistor followed by a fixed-gain stage, as shown in Figure 3.21. The output voltage, V_o, of this circuit is given by the following equation

$$V_o = G_1 G_2 V_i \tag{3.91}$$

where:

$$G_1 = \frac{R_{f1}}{R_{i1}},\ G_2 = \frac{R_{f2}}{R_{i2}}, \tag{3.92}$$

$$V_i = I_i R_{i1}, \tag{3.93}$$

G_1 and G_2 are the gain of the first and second amplifiers, R_{f1} and R_{f2} are the feedback resistor of the first and second amplifiers, R_{i1} and R_{i2} are the input resistor of the first and second amplifiers, respectively, V_i is the input voltage of the circuit, and I_i is the input current of the circuit. Substituting Equations 3.92 and 3.93 into Equation 3.91, the output voltage of the circuit is given by following equation

$$V_o = I_i \frac{R_{f1} R_{f2}}{R_{i2}} \tag{3.94}$$

3.5 Data Acquisition and Processing System

3.5.1 Description

Figure 3.22 shows a block diagram of the data acquisition and measurement system. This system consists of a fast relay multiplexer circuit, a sensitive electrometer amplifier circuit, and an analog to digital converter (detailed drawings are provided in Appendix B). The input current from the electrometer rings are sent to the reed relay multiplexer circuit for the channel selection via a series of a low-noise coaxial connection cable, and is sent to the sensitive electrometer amplifier in order to increase the level of the signal current. The electrometer amplifier is the simple current to voltage converter circuit. The output signal from the electrometer amplifier is in the range of 0 to +5V. It is then sent to a unipolar analog to digital converter (ADC), which is a 8-bit ADC, controlled by I^2C bus from the external personal computer or laptop via parallel port interface. The digital ADC signal is processed by computer software base on Microsoft Visual Basic programming. Figure 3.23 shows the EMS data acquisition and processing software.

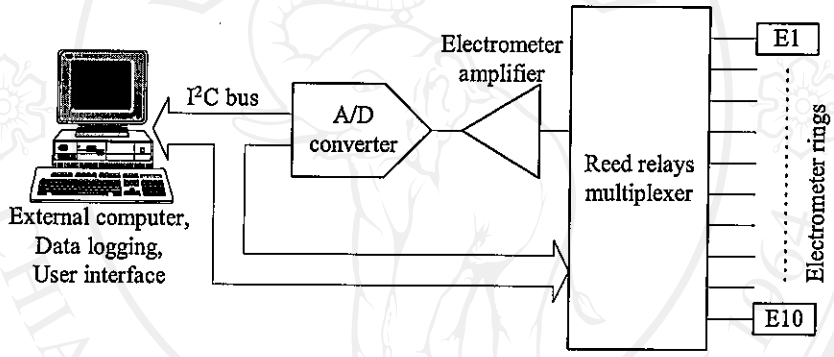

Figure 3.22 Block diagram of the data acquisition and processing system.

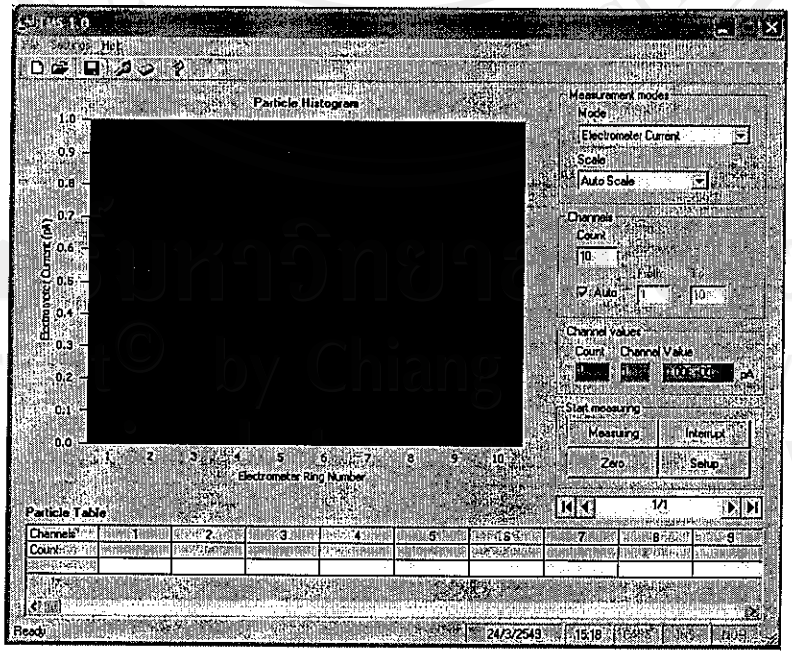

Figure 3.23 The EMS data acquisition and processing software.

3.5.2 Analytical Model

In this Section, approach to obtain the particle size distribution of aerosol from the measured signal current is provided. This is based on the measurement of the electric currents generated by charged particles drifting from the sample aerosol flow to the electrically isolated measuring electrode of the mobility analyzer which connected to a sensitive electrometer circuit (Whitby and Clark 1966; Tammet 1967; Israel 1970; Whitby 1976; Liu *et al.* 1979; Lehtimaki 1987; Mirme 1994; Tammet *et al.* 2001; Kulon *et al.* 2001; Graskow 2001; Biskos 2004). Deposition of charged particles on the measuring electrode will contribute to the measured signal current. The current measurements from the measuring electrode are then converted to particle number concentrations corresponding to the particle size collected on the electrode. If the mobility distribution function, $f(Z_p)$, is defined as

$$f(Z_p) = \frac{dN_p}{dZ_p} \tag{3.95}$$

where dN_p is the number concentration of aerosols in the mobility range dZ_p then the electric current of a singly charged particles, I_p, can be derived making use of the well known result that the rate at which particles are collected on the measuring electrode of the mobility analyzer is given by the following equation:

$$I_p = Qe\left(\int_{Z_c}^{\infty} f(Z_p)dZ_p + \frac{1}{Z_c}\int_0^{Z_c} Z_p f(Z_p)dZ_p \right) \tag{3.96}$$

where Q is the sample flow rate, e is the value of the elementary units of charge, Z_c is the critical mobility of the classifier is a function of the dimensions of the classifier, the applied voltage, and the flow rate of aerosol and sheath air, Z_p is the particle electrical mobility (i.e. particle drift velocity/field strength), and $f(Z_p)dZ_p$ is the number concentration of aerosol, N_p, with mobility between Z_p and $Z_p + dZ_p$. The above equation was originally derived by Tammet (1967) and Israel (1970). All particles with mobility, Z_p, higher than a critical mobility, Z_c, are collected on the measuring electrode and contribute to the measured current and are accounted for in the first term. But particles with mobility lower than the critical value are contributed to the measured current only in proportional to Z_p/Z_c is given by the second term.

For the present spectrometer, the principle of the current measuring technique in the classifier is shown in Figure 3.24. The signal current of a singly charged particles collected on the electrometer ring in channel i become

$$I_{p,i} = Q_a e\left(\int_{Z_{p,i}^{\min}}^{Z_{p,i}^{\max}} f(Z_p)dZ_p + \frac{1}{Z_{p,i}^{\min}}\int_0^{Z_{p,i}^{\min}} Z_p f(Z_p)dZ_p \right) \tag{3.97}$$

where $I_{p,i}$ is the electrometer signal current measured at channel i, and Q_a is the sample aerosol flow rate. Considering the critical mobility in the range of $Z_{p,i}^{\min} < Z_{p,i} < Z_{p,i}^{\max}$, all particle are measured. Therefore, the second term is not significant and the currents have the simple form as

$$I_{p,i} = Q_a e N_{p,i} \tag{3.98}$$

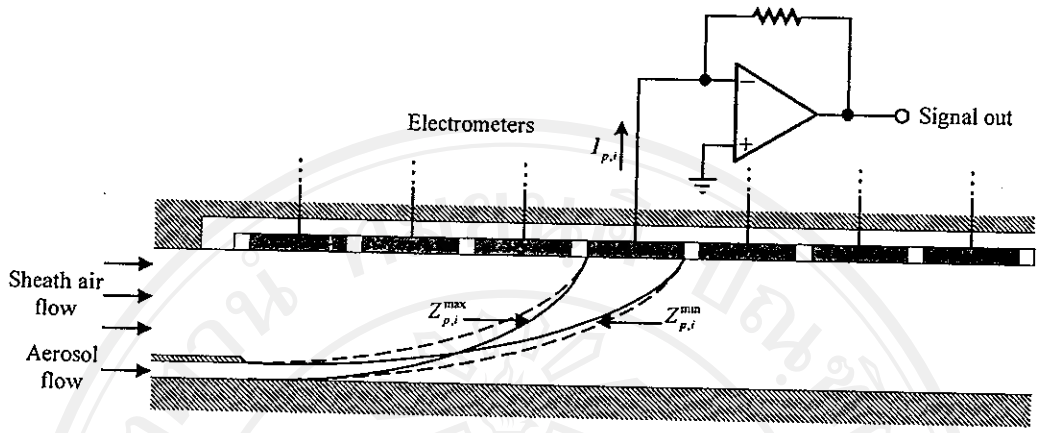

Figure 3.24 Principle of the current measuring technique in the classifier.

where $N_{p,i}$ is the particle number concentration at channel i. The signal current was then used to evaluate particle number concentration. Thus, the particle number concentration of particles, $N_{p,i}$, in the mobility range from $Z_{p,i}^{min} < Z_{p,i} < Z_{p,i}^{max}$ is related to the signal current, $I_{p,i}$, as follows:

$$N_{p,i} = \frac{I_{p,i}}{eQ_a} \tag{3.99}$$

In fact, the aerosol contains not only singly charged particles of the desired particle size, but also multiply charged particles of a larger particle size. Thus, the multiply charged particles must be applied to Equation 3.99, and can be rewritten to give

$$N_{p,i} = \frac{I_{p,i}}{n(d_{p,i})eQ_a} \tag{3.100}$$

where $n(d_{p,i})$ is the fraction of particles with diameter $d_{p,i}$ that carry n elementary charges. To obtain size distribution, the geometric midpoint diameter $d_{p,i}^{mid}$ is calculated as:

$$d_{p,i}^{mid} = \left(d_{p,i}^{min} d_{p,i}^{max}\right)^{1/2} \tag{3.101}$$

where $d_{p,i}^{min}$ is the particle diameter with minimum mobility in channel i, and $d_{p,i}^{max}$ is the particle diameter with maximum mobility in channel i. The geometric midpoint particle number concentration in channel i as:

$$N_{p,i} = \frac{I_{p,i}}{n(d_{p,i}^{mid})eQ_a} \tag{3.102}$$

The measured size channel i distribution results corresponds to the channel concentration $N_{p,i}$ divided by the channel geometric width as:

$$\frac{N_{p,i}}{d\log(d_{p,i})} = \frac{N_{p,i}(d_{p,i}^{\text{mid}})}{\log(d_{p,i}^{\max}/d_{p,i}^{\min})} \tag{3.103}$$

3.6 Summary

This Chapter has presented a detailed description of the EMS and the analytical and numerical models used to predict the performance of the individual components of the EMS. These include the size selective inlet, the particle charger, the mobility classifier, the electrometer and the data acquisition and processing system. Starting with the detailed description and the analysis of the size selective inlet we presented the approach used to calculate the acceleration nozzle diameter and the nozzle-to-plate distance from the Stokes number. Next, we gave the detailed description of the particle chargers and described the analytical theories for estimating the $N_i t$ product in the charging zone, the analytical theories used to estimate the particle penetration and charging rate. We also showed the numerical models used to investigate the flow and electric field in the charging zone of the charger. In the third Section, a detailed description of the mobility classifier was presented. Analytical and numerical models that estimate the particle trajectory with/without Brownian diffusion motion, the electrical mobility and size classification on the different electrometer rings along the classifier, flow field and electric field patterns in the classifier were also described in this Section. A detailed description and the analytical model of the electrometer circuit used to predict the output voltage were described in the fourth Section. Finally, we gave the data acquisition and processing system of the EMS and we showed how to calculate the particle size distribution of aerosols.